arXiv:1411.1269v1 [astro-ph.GA] 5 Nov 2014

Baltic Astronomy, vol.???, , ????

Ionized gas velocity dispersion and multiple supernova explosions

Evgenii O. Vasiliev[1,2], Alexei V. Moiseev[3,4] and Yuri A. Shchekinov[2]

[1] *Institute of Physics, Southern Federal University, Stachki Ave. 194, Rostov-on-Don, 344090 Russia; eugstar@mail.ru*

[2] *Department of Physics, Southern Federal University, Sorge Str. 5, Rostov-on-Don, 344090 Russia*

[3] *Special Astrophysical Observatory, RAS, Nizhnii Arkhyz, Karachaevo-Cherkesskaya Republic, 369167 Russia*

[4] *Sternberg Astronomical Institute, Moscow M.V. Lomonosov State University, Universitetskij pr., 13, 119992 Moscow, Russia*

Received: 20?? December 2; accepted: 20?? December 15

Abstract. Using 3D numerical simulations we study the evolution of the Hα intensity and velocity dispersion for single and multiple supenova (SN) explosions. We find that the $I_{\rm H\alpha}-\sigma$ diagram obtained for simulated gas flows is similar in shape to that observed in dwarf galaxies. We conclude that colliding SN shells with significant difference in age are resposible for high velocity dispersion that reaches values high as $\gtrsim 100$ km s^{-1}. Such a high velocity dispersion could be hardly got for a single SN remnant. Peaks of velocity dispersion on the $I_{\rm H\alpha}-\sigma$ diagram may correspond to several stand-alone or merged SN remnants with moderately different ages. The procedure of the spatial resolution degrading in the Hα intensity and velocity dispersion maps makes the simulated $I_{\rm H\alpha}-\sigma$ diagrams close to those observed in dwarf galaxies not only in shape, but also quantitatively.

Key words: galaxies: ISM – ISM: bubbles – shock waves – supernova remnants – kinematics and dynamics

1. INTRODUCTION

The 3D spectroscopy in optical emission lines yields a detailed information about the kinematics of the ionized gas in the interstellar medium (ISM) of external galaxies with a seeing-limited angular resolution. On one hand, it provides the angular resolution $1-3$ arcsec, that is an order of magnitude higher than that reached in radio observations. But on the other hand, it is limited by only to the regions around ionizing radiation sources, like OB stars, stellar winds and supernova explosions. Kinetic energy output from these objects may be responsible for driving turbulent motions in ambient gas and forming galactic outflows. The observed characteristic of these motions is a velocity dispersion σ determinated as a standard deviation of the Gaussian profile describing Balmer emission lines after accounting for the instrumental effects and subtracting the contribution of the natural and thermal broadening in the HII regions. For understanding observations of starforming complexes Muñoz-Tuñón et al. (1996) and Yang et al. (1996) have

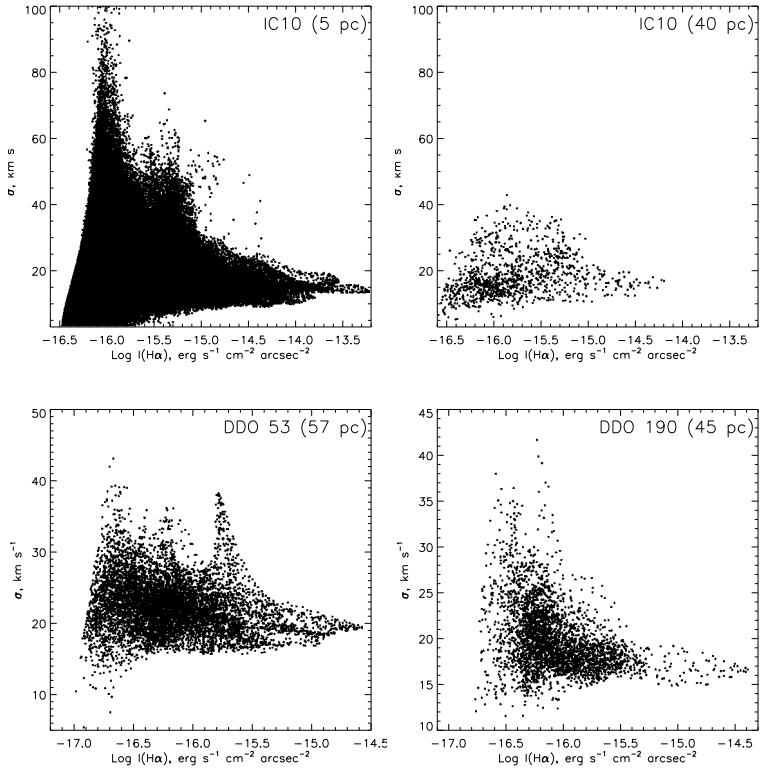

Fig. 1. The $I_{\mathrm{H}\alpha} - \sigma$ diagram for nearby dwarf galaxies according Moiseev & Lozinskaya (2012): IC 10 (original and smoothed data), DDO 53 and DDO 190. The spatial resolution is marked in the brackets.

proposed to use the relation between the Hα intensity (i.e. the emission line surface brightness) and velocity dispersion – the $I_{\mathrm{H}\alpha} - \sigma$ diagram. More recently Martínez-Delgado et al. (2007), Bordalo et al. (2009), Moiseev et al. (2010), Moiseev & Lozinskaya (2012) have considered $I_{\mathrm{H}\alpha} - \sigma$ diagrams to study the ionized gas in several dwarf galaxies. Figure 1 presents such diagrams for nearby dwarf irregular galaxies IC 10, DDO 190 and DDO 53. The observational data for these diagrams were obtained using a scanning Fabry-Perot interferometer with the 6-m telescope of the SAO RAS and described in details by Moiseev & Lozinskaya (2012). The spatial resolution in the observations of the nearest galaxy IC 10 (5 pc) is 8 times better than that for DDO 190 and DDO 53 galaxies. In observations with lower resolution gaseous motions in small HII regions, thin shells and colliding shocks are averaged with neighbouring low-velocity flows. So the data on the small-scale kinematics of gas is lost for two latter galaxies that are more distant than IC 10. To imitate the effect of low resolution, the original data cube for IC 10 was first smoothed by the two-dimensional Gaussians, and then binned, so that the resulting pixel size compared to that for DDO 190 and DDO 53 (Moiseev & Lozinskaya 2012). The diagram for IC 10 after degrading resolution looks similar to these for DDO 190 and DDO 53 and fills the same range of σ. In general, all such diagrams

have similar shape, because there are several main sources that contribute to Hα line intensity and that drive motions in turbulent ISM. Namely, there are HII regions, stellar winds and supenova remnants. Acting together they form multiphase turbulent ISM. Up-to-date only quantitive interpretation of $I_{\rm H\alpha} - \sigma$ diagrams were proposed by Muñoz-Tuñón et al. (1996). However one can be interested in how ionized gas has reached to the state, which corresponds to shape of $I_{\rm H\alpha} - \sigma$ diagrams observed in galaxies.

In this note we consider the evolution of the Hα intensity and velocity dispersion for single and multiple supenova explosions.

2. NUMERICAL MODEL

We are interested in the relation between emissivity in Hα line and velocity dispersion for gaseous flows driven by multiple SN explosions in starforming galaxies (the detailed study of multiple SNe dynamics can be found in Vasiliev et al. 2014). We follow the evolution of the Hα emission intensity and velocity dispersion in a small box of 200 pc^3. For SN rate we consider a finite number of SNe exploded each 10^5 and 10^4 yrs, which corresponds to the rate 1.25×10^{-12} and 1.25×10^{-11} pc^{-3} Myr^{-1} in case of continous starformation on galactic scales. For comparison we investigate how similar values evolve in case of single SN explosion.

We carry out 3-D hydrodynamic simulations (Cartesian geometry) of multiple/single SNe explosions. We take periodic boundary conditions. The computational domain has size 200^3 pc^3, which has 300^3 cells, corresponding to a physical cell size of 0.75 pc. The background number density considered are 0.1 and 1 cm^{-3}, and the background temperature is 10^4 K. The metallicity is constant within the computational domain (we do not consider here the mixing of metals ejected by SNe, this question will be studied in a separate work), and we consider cases with $Z = 0.1, 1$ Z$_\odot$. We inject the energy of each SN in the form of thermal energy in a region of radius $r_i = 1.5$ pc. The energy of each SN equals 10^{51} erg. SNe are distributed uniformly and randomly over the computational domain.

We use three-dimensional unsplit total variation diminishing (TVD) code based on the Monotonic Upstream-Centered Scheme for Conservation Laws (MUSCL)-Hancock scheme and the Haarten-Lax-van Leer-Contact (HLLC) method (e.g. Toro 1999) as approximate Riemann solver. This code has successfully passed the whole set of tests proposed in (Klingenberg et al. 2007).

In the energy equation we take into account cooling processes adopted the tabulated non-equilibrium cooling curve (Vasiliev 2013). This cooling rate is obtained for a gas cooled isobarically from 10^8 down to 10 K. The full description of our method of cooling rate calculations and the references to the atomic data can be found in (Vasiliev 2011, 2013). Briefly, the non-equilibrium calculation includes the ionization kinetics of all ionization states for the following chemical elements: H, He, C, N, O, Ne, Mg, Si, Fe as well as molecular hydrogen kinetics at $T < 10^4$ K. The heating rate is adopted to be constant, whose value is chosen so that the background gas does not cool. The stabilization vanishes when the density and temperature goes out of the narrow range near the equilibrium state.

We use the pre-computed cooling rates because the self-consistent calculation of cooling rates in multi-dimensional dynamics is a very time consuming task. In general, the evolution of gas behind shock waves with velocities higher than $\gtrsim 150$ km s^{-1} are very close to that of a gas cooled from very high tempera-

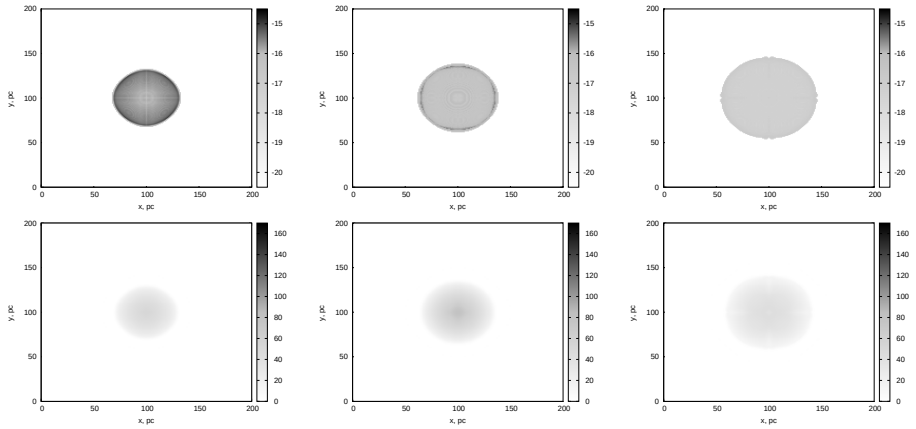

Fig. 2. The Hα intensity $I_{\rm H\alpha}$ (in erg cm^{-2} s^{-1} arcsec^{-2}) – top row, velocity dispersion (in km/s) maps – bottom row, for single SN explosion at $t = 0.1$, 0.2 and 0.4 Myr (from left to right columns).

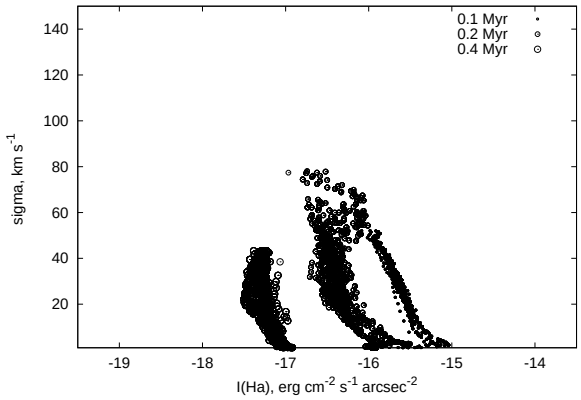

Fig. 3. The $I_{\rm H\alpha} - \sigma$ diagram for single SN explosion at $t = 0.1$, 0.2 and 0.4 Myr (from small to large symbols).

ture $T = 10^8$ K (e.g., Vasiliev 2012). Here we study multiple SN explosions, whose shells collide and merge with each other with typical velocities higher than 100 km s^{-1}.Therefore the non-equilibrium cooling rates can be pre-computed for a gas cooled from very high temperature, e.g. $T = 10^8$ K and these rates can be used to study SN shell evolution in tabulated form.

3. RESULTS

First of all to understand Hα emission and velocity dispersion distributions for multi-SNe explosions we consider these distributions for single SN exploded in homogeneous medium. Figure 2 shows the Hα intensity and velocity dispersion maps for three time moments. One can see the drop of the average intensity with time, and note that the velocity dispersion in the direction of the explosion center

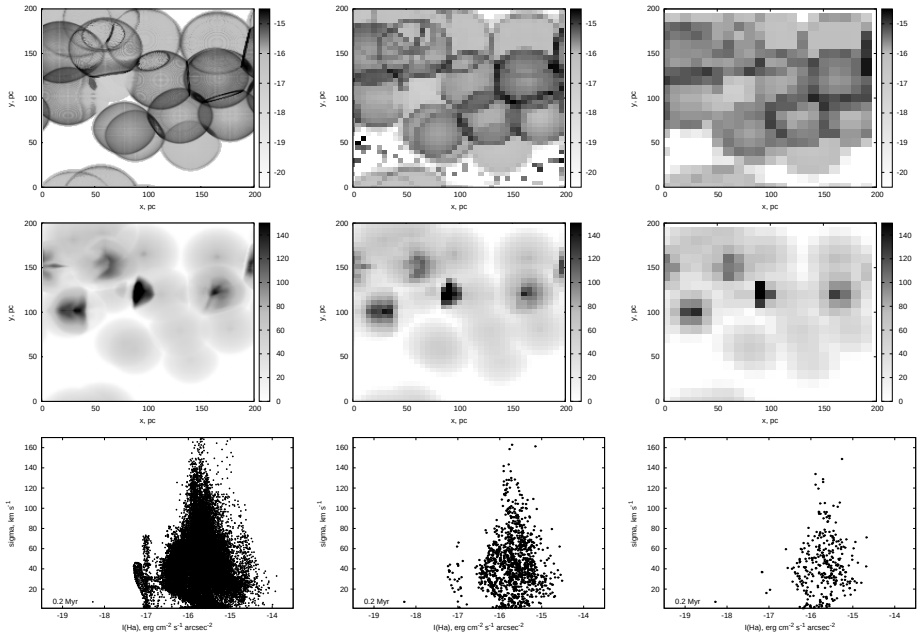

Fig. 4. The Hα intensity $I_{\mathrm{H}\alpha}$ (in erg cm^{-2} s^{-1} arcsec^{-2}) – top row, velocity dispersion (in km/s) maps – middle row, and $I_{\mathrm{H}\alpha} - \sigma$ diagram – bottom row, for SN rate 1.25×10^{-11} pc^{-3} Myr^{-1} at $t = 0.2$ Myr. The numerical data without degrading resolution procedure is shown in left column of panels, the smoothed and binned data are presented for $h = 2.5$ pc and $N = 5$ pc in middle column, $h = 5$ pc and $N = 10$ pc in right column.

grows at $t \sim 0.2$ Myr and than decreases. Around $t \sim 0.2$ Myr the reverse shock overtakes the blastwave due to decelerating the latter. Because of higher velocity of the reverse shock the velocity dispersion increases. After short interaction between shocks the dispersion drops monotonically in time. Figure 3 shows the $I_{\mathrm{H}\alpha} - \sigma$ diagram for single SN explosion. It is clearly seen that the locus of points corresponded to the same time moment shifts with time to region with lower Hα intensity. The maximum velocity dispersion is about 80 km s^{-1} reaches when the reverse shock is close to the blastwave. For older remnant the intensity and velocity dispersion becomes smaller. Decrease of the ambient density leads to longer evolution, but the maximum velocity dispersion after the beginnig of the radiation phase depends on the ambient density value slightly.

Figure 4 (left column of panels) presents the Hα intensity (upper), the velocity dispersion (middle) maps and the $I_{\mathrm{H}\alpha} - \sigma$ diagram (bottom) for SN rate 1.25×10^{-11} pc^{-3} Myr^{-1} at $t = 0.2$ Myr. Several SN bubbles are clearly identified (only two dozens SNe have exploded till this time), some of them interact between each other. It is clearly seen that high Hα intensity and velocity dispersion are associated with young SN remnants. But the highest velocity dispersion can be found around colliding shells of young and old SNe. A breakthrough of high velocity gas of young SN shell into warm rarefied interiors of the old SN produces a strong shock wave. So that we can conclude that collisions of SN shells with significant difference in age are resposible for velocity dispersion reaches the value

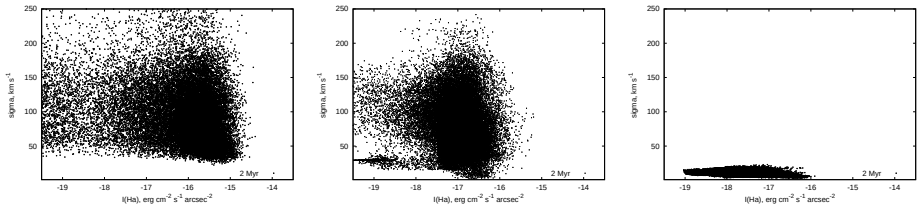

Fig. 5. The $I_{\rm H\alpha} - \sigma$ diagrams for continous SN explosions with rate 1.25×10^{-11} pc^{-3} Myr^{-1} (1 SN per 10^4 yrs in box 200 pc^3, left panel), 1.25×10^{-12} pc^{-3} Myr^{-1} (1 SN per 10^5 yrs in box 200 pc^3, middle panel) and for limited (15) number SNe with delay 10^4 yrs (right panel) at $t = 2$ Myr.

high as $\gtrsim 100$ km s^{-1}. When two shells of SN with similar ages collide, a cold layer with divergent shocks is formed, in this case the velocity dispersion value does not increase significantly. Several peaks of σ in the diagram conform to multiple stand-alone SN remnants with moderately different ages. Similar peaks can be found in dwarf galaxy DDO 53 (see Figure 1). For instance, similar picture takes place at $t \sim (3-5) \times 10^5$ yrs for SN explosions with frequency 1 per 10^5 yr, whose shells do not (or slightly) interact each other.

One can see that the $I_{\rm H\alpha} - \sigma$ diagram has a shape similar to observed one in dwarf galaxies after 10-20 SN explosions (several of them should collide each other) with frequency 1 per $\sim 10^4$ yr. Decrease of frequency (or, in general, SN rate) leads to smaller velocity dispersion. At further time the shape of $I_{\rm H\alpha} - \sigma$ diagram depends on whether SN exposions continue or stop. For the first case SN shell collisions lead to further increase of velocity dispersion, which can reach $\sim 200 - 250$ km s^{-1} (Figure 5, left and middle panels). Both rarefied and hot gas has high velocity dispersion, but low Hα intensity. Note that because the observed σ maps were masked by the fixed S/N level (the left-hand side boundary of the point cloud in the observed diagrams is due to such masking), such rarefied and hot gas cannot be detected in observations. Decrease of SN frequency shifts the point cloud to lower intensities (Figure 5, middle panel). For the case of limited SN number the SN shells lose their energy during ~ 1 Myr (in gas with $n = 0.1$ cm^{-3}) after the last SN has exploded, thus, both Hα intensity and velocity dispersion drop to negligible values (Figure 5, right panel).

Thus, the $I_{\rm H\alpha} - \sigma$ diagram obtained in our simulations is expected to be close to observed one, when (*i*) a starformation burst leads to 10-20 nearest SN explosions, (*ii*) several SN shells should collide, and (*iii*) the next burst will be not earlier than previous SN remnants cool down and merge with ISM. Note that the diagram has a shape like in observation only in several hundred thousands years after the burst has finished, so we can conclude that the last starformation episod in the observed galaxies, whose diagrams have similar shape, has taken place not earlier than several hundreds thousand years ago.

In observations the spatial resolution is much less than that in our simulations. To test our conclusions and compare our results with the observations we degrade the resolution of the Hα and velocity dispersion maps. We smooth the maps with 2D Gaussian filter of h size and after re-bin the smoothed maps with size of a bin equals to N. Figure 4 (middle and right columns of panels) presents the Hα intensity and the velocity dispersion after the degrading procedure. The maximum of velocity dispersion decreases from $\sim 160 - 170$ km s^{-1} in the original

map to $\sim 120 - 140$ km s^{-1} for $h = 5$ pc and $N = 5$ pc (middle column) and to $\sim 100 - 110$ km s^{-1} for $h = 10$ pc and $N = 10$ pc (right column), this spatial resolution is close to that in the observations of IC 10. So the velocity dispersion peak in the degraded $I_{\mathrm{H}\alpha} - \sigma$ diagrams has a magnitude similar to that observed in dwarf galaxies (Martínez-Delgado et al. 2007, Moiseev et al. 2010, Moiseev & Lozinskaya 2012) and the model points occupy the similar ranges of the Balmer lines surface brightness and line-of-sight velocity dispersion.

4. CONCLUSIONS

We have studied the Hα intensity – velocity dispersion diagram for single and multiple SNe. We found that the diagram obtained in our simulations are close in shape to those observed in the nearby dwarf galaxies. For single SN remnant the maximum velocity dispersion is about several dozens km s^{-1} and reaches it when the reverse shock is close to the blastwave. We concluded that collisions of SN shells with significant difference in age are resposible for high velocity dispersion that reaches values high as $\gtrsim 100$ km s^{-1}. Peaks of velocity dispersion on the $I_{\mathrm{H}\alpha} - \sigma$ diagram may correspond to several stand-alone or merged SN remnants with moderately different ages. Similar structures can be found at the diagrams for dwarf galaxy DDO 53. We investigated the decrease of spatial resolution on shape of $I_{\mathrm{H}\alpha} - \sigma$ diagrams. We found that the $I_{\mathrm{H}\alpha} - \sigma$ diagrams obtained after the procedure of degrading resolution not only retain its similarity in shape, but also become quantitatively close to those observed dwarf galaxies.

ACKNOWLEDGMENTS. EV and YuS thank to the RFBR for support (project codes 12-02-00365 and 12-02-00917). EV and AM is also grateful for the financial support of the non-profit "Dynasty" Foundation. EV thanks to the Ministry of Education and Science of the Russian Federation (project 213.01-11/2014-5). The work is partly supported by the Research Program OFN-17 of the Division of Physics, Russian Academy of Sciences.

REFERENCES

Bordalo V., Plana H., Telles E., 2009, ApJ, 696, 1668

Klingenberg Ch., Schmidt W., Waagan K., 2007, J. Comp. Phys., 227, 12

Martínez-Delgado I., Tenorio-Tagle G., Muñoz-Tuñón C., Moiseev A.V., Cairós L.M., 2007, AJ, 133, 2892

Moiseev A.V., Lozinskaya T.A., 2012, MNRAS, 423, 1831

Moiseev A.V., Pustilnik S.A., Kniazev A.Y., 2010, MNRAS, 405, 2453

Muñoz-Tuñón C., Tenorio-Tagle G., Castañeda H.O., Terlevich R., 1996, AJ, 112, 1636

Toro E., Riemann solvers and numerical methods for fluid dynamics. Springer-Verlag, Berlin, second edition, 1999. A practical introduction.

Vasiliev E.O., 2011, MNRAS, 414, 3145

Vasiliev E.O., 2012, MNRAS, 419, 3641

Vasiliev E.O., 2013, MNRAS, 431, 638

Vasiliev E.O., Nath B.B., Shchekinov Yu.A., 2014, MNRAS accepted, arXiv:1401.5070

Yang H., Chu Y-H., Skillman E. D., Terlevich R., 1996, AJ, 112, 146